Copy 5
RM A52F16

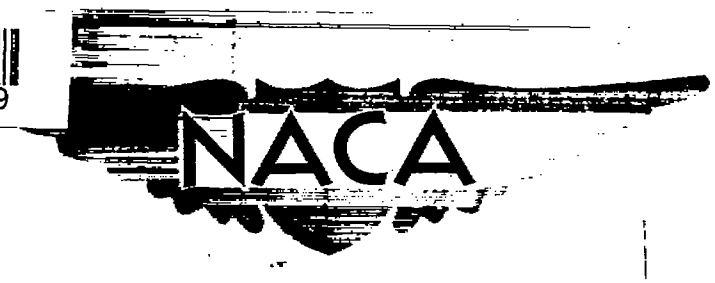

RESEARCH MEMORANDUM

EFFECT OF CAMBER AND TWIST ON THE STABILITY CHARACTERISTICS OF MODELS HAVING A 45° SWEPT WING AS DETERMINED BY THE FREE-FALL METHOD AT TRANSONIC SPEEDS

By Maurice D. White

Ames Aeronautical Laboratory
Moffett Field, Calif.

NATIONAL ADVISORY COMMITTEE
FOR AERONAUTICS

WASHINGTON
August 29, 1952

NATIONAL ADVISORY COMMITTEE FOR AERONAUTICS

RESEARCH MEMORANDUM

EFFECT OF CAMBER AND TWIST ON THE STABILITY CHARACTERISTICS OF MODELS HAVING A 45° SWEPT WING AS DETERMINED BY THE FREE-FALL METHOD AT TRANSONIC SPEEDS

By Maurice D. White

SUMMARY

Measurements were made in free fall at transonic speeds of the dynamic stability characteristics of three models. Two of the models had 45° swept wings of aspect ratio 6 and 45° swept tail surfaces, and differed from each other only in that the wing of one of the models was plane and the wing of the other was cambered and twisted. The third model had the same fuselage-tail arrangement as the others, but had no wing. Static and dynamic longitudinal stability characteristics of the models were determined at Mach numbers ranging from 0.84 to 1.16, wing Reynolds numbers ranging from 2,700,000 to about 6,000,000, and angles of attack from about zero lift to stalling angles at the lower Mach numbers, and to a maximum of 10° to 12° at the higher Mach numbers. The results showed no significant difference in the stability characteristics of the models due to cambering and twisting the wing. There was an appreciable variation in static longitudinal stability of the two wing-on models in traversing the Mach number range, with the maximum stability occurring at a Mach number of about 0.97. The static directional stability of the three models was relatively unaffected by Mach number variation.

INTRODUCTION

The prediction of the dynamic stability characteristics of airplanes or missiles is particularly difficult in the transonic speed range where theoretical methods are generally inadequate, and aerodynamic derivatives tend to change value rapidly or erratically with changing Mach number. References 1, 2, and 3 present experimentally determined variations of dynamic stability characteristics with Mach number which illustrate the erratic nature of the results in this region. Since it is apparent that experimental results for specific configurations will have to be relied

upon as the basis for design for some time to come, any information that can be added to the existing fund of data should be of value.

Some additional experimental data have been obtained on the dynamic stability characteristics of several models as part of an investigation that was made at Edwards Air Force Base by the Ames Laboratory of the NACA using the free-falling recoverable-body technique. The investigation was made to compare the characteristics of two models having high-aspect-ratio 45° swept wings, one plane and the other cambered and twisted. In addition, the same fuselage-tail arrangement was tested without a wing.

The tests covered a Mach number range from 0.84 to 1.16, and a wing Reynolds number range from 2,700,000 to about 6,000,000. The angles of attack ranged from about zero lift to stalling angles at the lower Mach numbers, and to a maximum of 10° to 12° at the higher Mach numbers.

NOTATION

a_x longitudinal acceleration, units of g

a_z vertical acceleration, units of g

a.c. aerodynamic center position, percent $\bar{c}$

b_w wing span, feet

c local wing chord, feet

c.g. center of gravity position, percent $\bar{c}$

$\bar{c}$ wing mean aerodynamic chord $\left(\dfrac{\int_0^{b_w/2} c^2 dy}{\int_0^{b_w/2} c\, dy}\right)$, feet

g acceleration of gravity, 32.2 feet per second squared

I_Y moment of inertia in pitch, slug-feet squared

l_t tail length, feet

m mass, slugs

M Mach number

[redacted]

P	period of oscillation, seconds
q	angular velocity in pitch, radians per second
q_o	dynamic pressure $\left(\frac{1}{2}\rho V^2\right)$, pounds per square foot
$\dot{q}$	$\frac{\partial q}{\partial t}$
r	ordinate of fuselage, inches
S	wing area, square feet
S_t	horizontal-tail area, square feet
t	time, seconds
$T_{1/2}$	time for oscillation to damp to one-half amplitude, seconds
V	velocity, feet per second
W	model weight, pounds
x	longitudinal station, inches
y	spanwise distance from plane of symmetry, feet
α	angle of attack, degrees
α_t	angle of attack of tail, degrees
α_T	trim angle of attack, degrees
$\dot{\alpha}$	$\frac{\partial \alpha}{\partial t}$, radians per second
β	angle of sideslip, degrees
δ	horizontal tail deflection, degrees
ϵ	angle of downwash, degrees
ρ	atmospheric density, slugs per cubic foot
η_t	tail efficiency
C_L	lift coefficient $\left(\frac{\text{lift}}{q_o S}\right)$

[redacted]

C_{L_t} lift coefficient of tail $\left(\frac{\text{lift}}{q_o S_t}\right)$

C_m pitching-moment coefficient of complete model about model center of gravity $\left(\frac{\text{moment}}{q_o S \bar{c}}\right)$

C_{m_w} pitching-moment coefficient of exposed wing panels $\left(\frac{\text{moment}}{q_o S \bar{c}}\right)$

$C_{n'}$ yawing-moment coefficient of complete model about model center of gravity $\left(\frac{\text{moment}}{q_o S \bar{c}}\right)$

C_{L_α} lift-curve slope $\left(\frac{\partial C_L}{\partial \alpha}\right)$, per degree

C_{m_α} pitching-moment-coefficient slope $\left(\frac{\partial C_m}{\partial \alpha}\right)$, per degree

C_{m_δ} control-surface effectiveness parameter $\left(\frac{\partial C_m}{\partial \delta}\right)$, per degree

C_{m_q} $\frac{\partial C_m}{\partial (q\bar{c}/2V)}$, per radian

$C_{m_{\dot{\alpha}}}$ $\frac{\partial C_m}{\partial (\dot{\alpha}\bar{c}/2V)}$, per radian

$C_{n_\beta'}$ yawing-moment-coefficient slope $\left(\frac{\partial C_{n'}}{\partial \beta}\right)$, per degree

MODEL

Three model configurations were tested, all having the same fuselage and tail-surface dimensions. Two of the configurations had wings and one had no wing. Figures 1 and 2 show a three-view drawing and a photograph of one of the winged configurations, and table I lists the physical specifications of the three models. The two winged models differed from each other only in that the wing of the plane wing model was symmetrical and untwisted, while the wing of the other model had camber and twist. For the model having the cambered and twisted wing, the washout of 10° at the tip (measured streamwise) was obtained by twisting the wing so that the constant-percent-chord lines remained straight. The wing was constructed of solid aluminum alloy.

The fuselage was 210.5 inches in length and had a fineness ratio of 12.4. The fuselage ordinates from the 8-inch to the 139.4-inch station are given by the equation in figure 1. From station 139.4 the fuselage tapered conically to a radius of 5.2 inches at station 189.6. From stations 189.6 to 210.5, a tail shape approximating that given by the equation for values of x from 183.1 to 204 was used.

Both of the horizontal-tail surfaces and both of the vertical-tail surfaces of each model were all-movable, pivoting on axes perpendicular to the fuselage axis. A schedule of horizontal-tail movement was preset so that the tails would deflect and return to trim position in rapid pulse-type movements at regular time intervals during the test phase of the drop. The vertical-tail surfaces were actuated differentially by the roll-position stabilization system to provide roll control. All the tail surfaces were constructed of solid aluminum alloy.

INSTRUMENTATION

NACA continuously recording flight instruments were used to record the various quantities measured. A listing of the quantities and of the instruments used to measure them follows:

Quantity	Instrument
Angle of attack and angle of sideslip	Slave selsyns or recording oscillographs (depending on the installation) recording movements of vanes mounted on boom ahead of body (fig. 1)
Rate of pitch and rate of roll	NACA turnmeter
Angular acceleration in pitch	Angular accelerometer with recording oscillograph
Vertical and longitudinal accelerations	Linear accelerometers with recording oscillograph and NACA 3-component accelerometer
Transverse acceleration	NACA 3-component accelerometer
Horizontal- and vertical-tail deflections	NACA 2-component control position recorder
Mach number and dynamic pressure	NACA 6-cell manometer

[redacted]

The airspeed system was calibrated at different angles of attack using the SCR 584 radar installation of the NACA High-Speed Research Station at Edwards Air Force Base. All the flight records were synchronized by means of a chronometric timer.

TESTS

The results presented in this report were obtained during a series of free-fall drops of the models in which the models were trimmed at different angles of attack and longitudinal disturbances were produced by intermittent movement of the horizontal-tail surfaces. The models were released from a carrier airplane at an altitude of 40,000 feet and allowed to fall freely at about zero lift attitude until the desired Mach number was reached. At that time the horizontal tail was moved abruptly to the setting for trim and, thenceforth, was pulsed at intervals of 2.4 seconds. A typical time-history plot of the control deflections and the resultant motions of the model for a portion of a flight is shown in figure 3. The results presented herein were obtained from analysis of the free-oscillation characteristics following each pulse. At the conclusion of the test periods of each drop, the models were recovered by the use of a dive brake and parachute.

The models were roll-position stabilized throughout the drop. The system employed stabilized the model within bank angles of approximately 10°, and within roll rates of about 0.9 radian per second.

The airspeed system of the models was calibrated throughout the test range using the NACA radar-phototheodolite method.

For the winged models, angles of attack ranging from about zero lift to the stall were covered for Mach numbers up to about 0.9; at higher Mach numbers angles of attack up to 10° were covered for the plane-wing model, and up to 12° for the cambered- and twisted-wing model. For the wing-off model, the results were obtained for angles of attack ranging from about -1° to 6°.

Generally, the angle-of-attack range covered by the oscillations during a drop was of the order of $\pm 4^\circ$. For the plane-wing models the range of angles covered at lower Mach numbers increased to as much as $\pm 7^\circ$ for one of the drops.

For the winged models a Mach number range from 0.84 to 1.10 was covered with Reynolds numbers ranging from 2,750,000 at the lower Mach number to 5,600,000 at the higher Mach number. For the wing-off model the Mach numbers ranged from 0.98 to 1.16 with Reynolds numbers (based on the wing mean aerodynamic chord) ranging from 3,900,000 to 6,250,000.

ACCURACY

Based on the uncertainties that are estimated to have been present in the various component quantities, it is believed that the accuracy of a single determination of any quantity is as noted below:

α	$\pm 1/4^{\circ}$
C_{l_α}	±0.005 (for linear range of angles of attack)
C_{m_α}	±0.012
a.c. position	$\pm 0.16\bar{c}$
$C_{m_q} + C_{m_{\dot{\alpha}}}$	±30 percent of actual value
C_{n_β}'	±0.003
C_{m_δ}	±0.02

ANALYSIS

Following the treatment used by other investigators, the flight data have been analyzed under the assumption that the motions of the body are adequately described by a linear second-order system. A detailed description of the method of analysis used is given in appendix A. Reference 4 presents a fairly complete discussion of this method of analysis and of the assumptions involved in its use.

For some of the data included in this report, the assumptions of linearity inherent in the methods of analysis have been violated. Aside from the fact that the data have been obtained generally under conditions of changing Mach number, dynamic pressure, and altitude, some of the oscillations encompassed ranges of angle of attack for which the lift coefficient and pitching-moment coefficient did not vary linearly with angle of attack.

It is apparent that the degree to which the effects of such nonlinearities will be evidenced in the final results will depend on the degree of nonlinearity present. No attempt is made in this report to analyze the data quantitatively in terms of the degree of nonlinearity.

RESULTS AND DISCUSSION

Lift

Figure 4 shows the variation of lift coefficient with angle of attack at different Mach numbers for the three model configurations with different control settings. A significant feature of these curves is the decrease in slope that is evidenced by the curves for the wing-on models at the higher angles of attack. This characteristic is particularly evident at the lower test Mach numbers ($M < 0.96$).

In figure 5 the lift-curve slopes for small angles of attack as determined from the data of figure 4 are presented as a function of Mach number. The curves of C_{L_α} for the two wing-on models show a general tendency to decrease with increasing Mach number through the test range. At the two extremes of the Mach number range the values for the two wings are in agreement, and at intermediate Mach numbers the values of C_{L_α} for the plane-wing model appear to be only slightly greater than those for the cambered- and twisted-wing model. Measurements of the forces on the exposed wing panels as determined from a balance within the fuselage show trends that essentially parallel those described above, which indicates that the variations are due primarily to the wings.

For the wingless model the lift-curve slope decreased generally with increasing Mach number between $M = 0.98$ and 1.16.

Longitudinal Trim

The trim angles of attack for all the drops were determined as the mean angle of attack of the oscillations. The variations with Mach number of the trim angles of attack as determined by this method are shown in figure 6 for all the drops. The results show the variations of trim angle of attack with Mach number to be generally small throughout the test range for all the models. Some increase in the variation of trim angle of attack with control deflection is noted at the lower Mach numbers. This is due largely to the decreased static stability which existed at these Mach numbers, rather than to increased control effectiveness.

Static Longitudinal Stability

Presentation of results.- The values of the static stability parameter C_{m_α} were determined from the half-periods of the oscillations,

as described in appendix A, and are shown in figure 7 as a function of Mach number for each of the configurations. In evaluating the results it was found that the variations of period with time following successive control disturbances did not always form a continuous curve. The causes of this phenomenon are still under investigation.

For presentation in figure 7 mean lines were drawn through all the data points following each control deflection and these curves were plotted as a function of Mach number. Each short line in figure 7 represents the variation of C_{m_α} following a control movement. This method of presentation illustrates the discontinuous nature of the data which was described above and shows also the variation of Mach number during the interval following a control disturbance. A mean line drawn through the short curves appears to indicate some of the larger trends of the data, even though small changes cannot be accurately identified.

As a result of operation of the roll stabilization system, variations in rolling velocity occurred during the oscillations with the maximum roll rates reaching values as large as 0.9 radian per second. Calculations based on reference 5 using measured frequencies in pitch and yaw indicate that a steady rate of roll of 0.9 radian per second would affect the value of C_{m_α} by only about 5 percent. Whether the effects of the oscillatory roll actually experienced would be greater or less remains to be established.

The faired curves of C_{m_α} in figure 7 were combined with effective values of C_{L_α} for the particular data to compute the aerodynamic center variations plotted in figure 8.

Effect of Mach number.- For the wingless model the negative values of C_{m_α} decreased progressively with increasing Mach number over the entire test range of Mach numbers despite the rearward movement of the aerodynamic center position that occurred over part of the Mach number range ($M = 1.06$ to $M = 1.16$). The decrease in lift-curve slope that occurred over this range (21 percent decrease between $M = 1.06$ and $M = 1.16$) was apparently great enough to more than offset the effect of the aerodynamic center movement.

The variations of C_{m_α} and aerodynamic center position with Mach number were of the same general character for both the winged models at small angles of attack. The values of C_{m_α} increased negatively with a corresponding rearward movement in aerodynamic center position as the Mach number was increased up to about $M = 0.98$. As the Mach number increased further and the aerodynamic center moved slightly forward, the values of C_{m_α} decreased negatively. The differences in variation of C_{m_α} between the cambered- and twisted-wing and plane-wing models were somewhat obscured by the scatter of the data. The range of values of C_{m_α} covered by the two winged models, however, appeared to be

essentially the same and somewhat greater than that noted for the wingless body over the restricted Mach number range for which comparisons could be made.

Effect of angle of attack.- As may be seen from figure 6 a number of tests were made in which the oscillations centered around different angles of attack. The results in figure 7 indicate that except at Mach numbers below $M = 0.92$ (with corresponding Reynolds numbers below 3,300,000) no large or consistent effects of angle of attack could be distinguished in the data. At the Mach numbers below $M = 0.92$ the data indicate a difference in the variation of C_{m_α} with angle of attack for the two winged models; that is, for oscillations covering high angles of attack, the cambered- and twisted-wing model showed an apparent decrease in negative value of C_{m_α}, while the plane-wing model showed an apparent increase. This difference in behavior is probably associated with the facts that (1) the angle-of-attack ranges designated as high and low were not the same for the two models, and (2) the variations of C_m with α were nonlinear at these Mach numbers. Figure 9 shows, at two Mach numbers, the variation of pitching-moment coefficient with angle of attack for the exposed wing panel as measured by a balance within the fuselage. In figure 9 letters are appended to the curves for $M = 0.86$ to identify the ranges of angles of attack covered in particular oscillations, and in figure 7 the stability data associated with these angles of attack are denoted by the same letters; that is, the curve labelled A-B in figure 7(b) represents data obtained from an oscillation between the angles of attack indicated by the letters A and B in figure 9(a), etc. It is apparent from the data of figure 9 that, whereas the oscillations of the cambered- and twisted-wing model covered two ranges of angles of attack in which the slopes of C_{m_w} were distinctly different (E-F and G-H), the oscillations of the plane-wing model covered ranges of angles of attack over which the variation of C_{m_w} was extremely nonlinear for both oscillations (A-B and C-D). For the latter cases it would be difficult to assign effective values of $C_{m_{\alpha_w}}$ to either the low- or the high-angle-of-attack oscillations, and it would therefore not be surprising if either an apparent increase or decrease in negative value of C_{m_α} were indicated for the higher angles of attack.

It is noteworthy that at the higher Mach numbers where no consistent differences due to angle of attack were evidenced by the oscillation data of figure 7, the wing-panel moment-coefficient data of figure 9 also showed little change in slope with angle of attack. The data for $M = 1.02$ in figure 9 illustrate the relative linearity of the variations of C_{m_w} with α at higher Mach numbers.

Damping in Pitch

The values of the damping-in-pitch parameter, $C_{m_q} + C_{m_{\dot{\alpha}}}$, determined by the method outlined in appendix A, are plotted as a function of Mach number for the three test configurations in figure 10. For comparison with the experimental results, values of $C_{m_q} + C_{m_{\dot{\alpha}}}$ estimated as described in appendix B are shown in the figures.

For the wingless body the data in figure 10(a) indicate that there is little variation in the value of $C_{m_q} + C_{m_{\dot{\alpha}}}$ as the Mach number is increased between $M = 0.98$ and $M = 1.16$. The estimated values were in good agreement with the experimental values throughout the test range of Mach numbers.

For the wing-on models figures 10(b) and 10(c) show that at Mach numbers above $M = 1.0$ the experimental values of $C_{m_q} + C_{m_{\dot{\alpha}}}$ for the two models were in essential agreement, both curves showing a slight decrease in value with increasing Mach number. For Mach numbers less than $M = 0.96$ there was a considerable difference in the level of the values of $C_{m_q} + C_{m_{\dot{\alpha}}}$ for the two models, although the variation with Mach number for the two models was about the same. This difference between the experimental values for the two models is associated with flight conditions for which greater nonlinearities in lift curves occurred for the plane-wing model than for the cambered- and twisted-wing model. (See fig. 4.) Since the value assumed for the lift-curve slope directly affects the experimentally determined value of $C_{m_q} + C_{m_{\dot{\alpha}}}$ (see appendix A), it is possible that the procedure employed here in evaluating the nonlinear lift-curve slope, that is, taking the average slope over the appropriate angle of attack range, gives the damping effect of a nonlinear lift-curve slope less weight than it deserves. However, even the assumption of a value of the lift-curve slope equal to that obtained at small angles of attack would not completely eliminate the differences between the two models. It would appear, therefore, that there are other differences in the characteristics of the models which are associated with the nonlinear lift curves and which affect the values of $C_{m_q} + C_{m_{\dot{\alpha}}}$.

For both the wing-on models there appeared to be a localized decrease in the value of $C_{m_q} + C_{m_{\dot{\alpha}}}$ which occurred at a Mach number of 0.96 for the plane-wing model and 0.98 for the cambered- and twisted-wing model. These Mach numbers, incidentally, correspond respectively to the Mach numbers where the static stability parameter C_{m_α} reached a peak (fig. 7). This local decrease in value of $C_{m_q} + C_{m_{\dot{\alpha}}}$ has been experienced in tests of other swept-wing models (reference 2) and, while of relatively small magnitude for the present models, might be of appreciable significance for airplanes having more conventional tail volumes.

Comparison of the estimated values of $C_{m_q} + C_{m_{\dot{\alpha}}}$ with the experimental values for the two wing-on configurations shows reasonably good agreement for the cambered- and twisted-wing model throughout the Mach number range and for the plane-wing model for Mach numbers above M = 0.98. For the plane-wing model the predicted values are considerably less than the experimental values for Mach numbers less than 0.94. The possible reason for this latter discrepancy has already been discussed as being at least partly due to the nonlinear lift-curve slopes.

Control-Surface Effectiveness

Values of the control-surface effectiveness parameter $\partial C_m/\partial \delta$ as determined by the method shown in appendix A are plotted in figure 11 as a function of Mach number. Data are shown only for the winged models over a limited range of Mach numbers. Results for the wing-off model were not included in figure 11 because they were based on data for only one drop and were therefore considered too inaccurate to be compared with the data for the wing-on models.

The results were consistent for the two winged models and, except for the decrease in value indicated at a Mach number of 0.94, the variation with Mach number is similar to the variation in lift-curve slope that occurs for 45° swept surfaces over this Mach number range.

Directional Stability

In some of the tests well-defined directional oscillations were indicated in the sideslip-angle records. These oscillations which were of usable regularity only for the smaller angles of attack were analyzed as described in appendix A to obtain the values of the static directional stability parameter, C_{n_β}', shown in figure 12. For comparison with these results the values of C_{m_α} for the wing-off configuration from figure 7 are also shown. The results show that the values of C_{n_β}' are much smaller than the values of C_{m_α} for the wing-off configuration. This would be anticipated as a result of the vertical tail being smaller in size than the horizontal tail. The curves of C_{n_β}' show no large variations with Mach number for any of the configurations.

Comparison of the values of C_{n_β}' for the various configurations showed the cambered- and twisted-wing model to have greater directional stability than either of the other models for Mach numbers less than about 0.9.

CONCLUDING REMARKS

Free-fall drop tests of three models at transonic Mach numbers indicated the following:

1. There was little difference throughout the Mach number range in either the static or dynamic longitudinal stability characteristics of two 45° swept-wing models, one having a cambered and twisted wing and the other a plane wing.

2. There was an appreciable variation in static longitudinal stability of the two wing-on models in traversing the Mach number range with the maximum stability occurring at a Mach number of about 0.97.

3. For the test technique employed, which consisted of pulsing the longitudinal control at regular time intervals, the variations with Mach number of the periods of the short-period oscillations were not continuous. The causes of this behavior are not yet established.

4. The variation of static directional stability with Mach number was small for the small angles of attack at which results were obtained. The cambered- and twisted-wing model appeared to have greater directional stability than the other models for Mach numbers less than about 0.9.

Ames Aeronautical Laboratory
National Advisory Committee for Aeronautics
Moffett Field, Calif.

APPENDIX A

ANALYSIS OF FLIGHT DATA

Equations of Motion

The results in the present investigation were analyzed by assuming that the following equations describe the motions of the model completely:

$$I_Y\dot{q} = M_\alpha\alpha + M_q q + M_{\dot{\alpha}}\dot{\alpha} + M_\delta\delta \tag{1}$$

$$mV(\dot{\alpha} - q) = -L_\alpha\alpha - L_\delta\delta \tag{2}$$

Combining these equations, the relationship is obtained that

$$\frac{q}{\delta} = \frac{C_o + C_1 D}{D^2 + bD + k} \tag{3}$$

where the constants C_o, C_1, b, and k are defined by the equations

$$C_o = \frac{M_\delta L_\alpha - L_\delta M_\alpha}{mVI_Y}$$

$$C_1 = \frac{M_\delta}{I_Y} - \frac{L_\delta M_{\dot{\alpha}}}{mVI_Y}$$

$$b = \frac{L_\alpha}{mV} - \frac{M_q + M_{\dot{\alpha}}}{I_Y}$$

$$k = -\frac{M_\alpha}{I_Y} - \frac{L_\alpha M_q}{mVI_Y}$$

and where

$$M_\delta = \frac{\partial C_m}{\partial \delta} 57.3 q_o S\bar{c}$$

$$L_\alpha = \frac{\partial C_L}{\partial \alpha} 57.3 q_o S$$

$$M_\alpha = \frac{\partial C_m}{\partial \alpha} 57.3 q_o S\bar{c}$$

$$L_\delta = \frac{\partial C_L}{\partial \delta} 57.3 q_o S$$

$$M_{\dot{\alpha}} = \frac{\partial C_m}{\partial\left(\frac{\dot{\alpha}\bar{c}}{2V}\right)} q_o S\bar{c} \frac{\bar{c}}{2V}$$

$$M_q = \frac{\partial C_m}{\partial\left(\frac{q\bar{c}}{2V}\right)} q_o S\bar{c} \frac{\bar{c}}{2V}$$

The denominator of equation (3) defines the control-fixed oscillatory characteristics of the model, the constant b being related to the damping of the oscillation by the expression

$$b = \frac{1.386}{T_{1/2}}$$

and the constant k, to the period of the oscillation by the expression

$$P = \frac{2\pi}{\sqrt{k - \left(\frac{b}{2}\right)^2}}$$

Evaluation of Flight Data

The detailed procedures used in evaluating the various quantities discussed in this report are described in the following paragraphs.

Lift-curve slope, C_{L_α}.- In order to evaluate the lift-curve slope C_{L_α}, time histories were made of the factors α and

$$C_L = \frac{W}{q_o S}\left(a_z \cos\alpha - a_x \sin\alpha\right)$$

For each of a number of values of α, C_L was determined and plotted against Mach number. For selected Mach numbers, faired values of C_L were determined from these plots and were plotted against the corresponding angles of attack.

Static stability parameter, C_{m_α}.- Considering only the regions where the longitudinal control was held fixed, measurements were made of the time intervals between successive peaks of the short-period oscillations. These measurements were made on four different records (q, $\dot{q}$, a_z, and α), and the values were plotted as a function of time and were faired. Values of the dynamic pressure q_o were also plotted as a function of time. Finally, at sufficient points to define the particular curves, the values of C_{m_α} were computed using the relation

$$C_{m_\alpha} = -\frac{\pi^2 I_Y}{57.3 S\bar{c}} \frac{1}{q_o\left(\frac{P}{2}\right)^2}$$

In the cases where the control moved despite efforts to fix it, the movement was found to be roughly in phase with the angle of attack and a correction was applied to the value of C_{m_α} as follows:

$$\Delta C_{m_\alpha} = \frac{\partial C_m}{\partial \delta} \frac{d\delta}{d\alpha}$$

where $\partial C_m/\partial \delta$ was determined from the test data, and the values of $d\delta/d\alpha$ from flight measurements.

The results from tests made with different center-of-gravity locations were converted to one center-of-gravity location by applying a correction

$$\Delta C_{m_\alpha} = \frac{[(c.g.)_{test} - (c.g.)_o]}{100} C_{L_\alpha}$$

The assumptions implicit in the procedure of analyzing the data by the methods described above are discussed in reference 4. These include the assumption that the equation of motion along the longitudinal axis may be ignored, and that certain terms may be ignored in the equations with little error. The errors in C_{m_α} due (1) to ignoring the term $(b/2)^2$ in the equation

$$P = \frac{2\pi}{\sqrt{k - \left(\frac{b}{2}\right)^2}}$$

and (2) to ignoring the term $\frac{L_\alpha M_q}{mVI_Y}$ in the equation

$$k = -\frac{L_\alpha M_q}{mVI_Y} - \frac{M_\alpha}{I_Y}$$

are at the most 3 percent and 2 percent, respectively.

Aerodynamic center position, a.c.- The aerodynamic center position was calculated as a fraction of the mean aerodynamic chord by using the equation

$$a.c. = 0.24 - \left(\frac{\partial C_m/\partial \alpha}{\partial C_L/\partial \alpha}\right)$$

where $\partial C_m/\partial \alpha$ was obtained from the faired curves of figure 7, and the effective values of $\partial C_L/\partial \alpha$ for the appropriate angle-of-attack ranges were used.

[redacted]

Damping in pitch parameter, $C_{m_q} + C_{m_{\dot{\alpha}}}$.- To evaluate the damping in pitch parameter $C_{m_q} + C_{m_{\dot{\alpha}}}$, semilog plots were made of the peak values of pitching velocity as a function of time, disregarding the algebraic signs of the values, and using values only from the regions where the longitudinal control was held fixed. From these plots, the values of the time required for the oscillation to damp to one-half amplitude, $T_{1/2}$, were obtained and applied in the equation

$$C_{m_q} + C_{m_{\dot{\alpha}}} = \frac{2I_Y V}{q_o S \bar{c}^2}\left(57.3 C_{L_\alpha} \frac{q_o}{V} \frac{S}{m} - \frac{1.386}{T_{1/2}}\right)$$

In this equation, the average value of C_{L_α} over the angle-of-attack range covered by the particular oscillations was employed.

Control effectiveness parameter, C_{m_δ}.- Values of C_{m_δ} were determined from the expression

$$\frac{\partial C_m}{\partial \delta} = \frac{\partial C_m}{\partial \alpha} \frac{\partial \alpha_T}{\partial \delta}$$

Static directional stability, $C_{n_\beta}{}'$.- The procedure for determining the values of $C_{n_\beta}{}'$ was similar to that described previously for determining C_{m_α}, differing only in that the sideslip-angle records were used to estimate the periods of the short-period oscillations. In order to permit direct comparison with the value of C_{m_α} for the wing-off model, the coefficient $C_{n_\beta}{}'$ is based on the wing mean aerodynamic chord instead of the wing span which is used conventionally.

APPENDIX B

ESTIMATION OF $C_{m_q} + C_{m_{\dot{\alpha}}}$

The methods used to estimate the values of the parameter $C_{m_q} + C_{m_{\dot{\alpha}}}$ are described in the following paragraphs.

Horizontal Tail

The contribution of the horizontal tail to the value of $C_{m_q} + C_{m_{\dot{\alpha}}}$ was estimated using the expression

$$C_{m_q} + C_{m_{\dot{\alpha}}} = 2 \frac{\partial C_{L_t}}{\partial \alpha_t} \eta_t \frac{l_t^2 S_t}{\bar{c}^2 S} \left(1 + \frac{d\epsilon}{d\alpha}\right)$$

The variation of $(\partial C_{L_t}/\partial \alpha_t)$ with Mach number assumed for the calculations was estimated from available wind-tunnel data and is shown in figure 13. The value of η_t was assumed to be 1.0 for the wing-off model and 0.9 for the wing-on models. The factor $1 + \frac{\partial \epsilon}{\partial \alpha}$ was considered equal to 1.0 for the wing-off model while, for the wing-on models, the variation with Mach number shown in figure 13 was obtained by interpolating data from references 6 and 7.

Fuselage

The method of reference 8 was used to estimate the contribution of the fuselage to the value of $C_{m_q} + C_{m_{\dot{\alpha}}}$. Using this method, it was found that the fuselage contribution was reasonably close to the rough figure used by other investigators (reference 2) of 25 percent of the tail contribution.

Wing

There appears to be no good theory available for predicting the contribution of the wing alone to the value of $C_{m_q} + C_{m_{\dot{\alpha}}}$ at transonic speeds. The trends of available supersonic theory indicate that the values would be quite small at the Mach numbers covered in these tests, and this contribution was, therefore, ignored in the estimations.

REFERENCES

1. Langley Pilotless Aircraft Research Division: Some Recent Data from Flight Tests of Rocket-Powered Models. NACA RM L50K24, 1951.

2. Triplett, William C., and Van Dyke, Rudolph D., Jr.: Preliminary Flight Investigation of the Dynamic Longitudinal-Stability Characteristics of a 35° Swept-Wing Airplane. NACA RM A50J09a, 1950.

3. Angle, Ellwyn E., and Holleman, Euclid C.: Determination of Longitudinal Stability of the Bell X-1 Airplane From Transient Responses at Mach Numbers up to 1.12 at Lift Coefficients of 0.3 and 0.6. NACA RM L50I06a, 1950.

4. Gillis, Clarence L., Peck, Robert F., and Vitale, A. James: Preliminary Results from a Free-Flight Investigation at Transonic and Supersonic Speeds of the Longitudinal Stability and Control Characteristics of an Airplane Configuration with a Thin Straight Wing of Aspect Ratio 3. NACA RM L9K25a, 1950.

5. Phillips, William H.: Effect of Steady Rolling on Longitudinal and Directional Stability. NACA TN 1627, 1948.

6. Goodson, Kenneth W., and Few, Albert G., Jr.: Aerodynamic Characteristics of a Wing with Quarter-Chord Line Swept Back 45°, Aspect Ratio 6, Taper Ratio 0.6, and NACA 65A006 Airfoil Section. Transonic-Bump Method. NACA RM L9I08, 1949.

7. Spreemann, Kenneth P., Morrison, William D., Jr., and Pasteur, Thomas B., Jr.: Aerodynamic Characteristics of a Wing with Quarter-Chord Line Swept Back 45°, Aspect Ratio 6, Taper Ratio 0.6, and NACA 65A009 Airfoil Section. Transonic-Bump Method. NACA RM L50B03a, 1950.

8. Smith, C. B., and Beane, Beverly J.: Damping in Pitch of Bodies of Revolution at Supersonic Speeds. IAS Preprint No. 311, 1951.

TABLE I.- DIMENSIONS OF FREE-FALL MODELS[1]

Gross weight, pounds[2]	1238 to 1356
Moment of inertia, slug-feet squared[2]	570 to 595
Center of gravity[2]	Station 100.2 or 101.3
Wing	
Area, square feet	9.0
Aspect ratio	6.0
Taper ratio	0.5
Sweepback, quarter-chord line, degrees	45
Span, feet	7.33
Mean aerodynamic chord, feet	1.27
Root chord, feet	1.64
Tip chord, feet	0.82
Airfoil section, perpendicular to quarter-chord line	
Plane wing	NACA 64A010
Cambered and twisted wing	NACA 64A810, a=0.8 (modified)
Twist, degrees washout at tip, measured streamwise	
Plane wing	0
Cambered and twisted wing	10
Incidence, degrees	+0.2
Horizontal tail (all-movable, pivoting about axis perpendicular to plane of symmetry of model)	
Area (including 2.0 square feet included in fuselage), square feet	6.0
Aspect ratio	4.3
Taper ratio	0.20
Sweepback, quarter-chord line, degrees	45
Span, feet	5.12

[1]Except as noted in the table, the wings of the two winged models were similar. The fuselage-tail configuration of all the models were the same.

[2]Two bodies of identical shape but different weight distribution were used. The plane-wing panels and the cambered- and twisted-wing panels were interchanged between the bodies during the test program so that the different weights and center-of-gravity positions are not readily identifiable with particular results.

TABLE I.- CONTINUED

Horizontal tail (continued)	
Mean aerodynamic chord (including area included in fuselage), feet	1.36
Leading edge of mean aerodynamic chord	Station 153.6
Root chord, feet	1.96
Tip chord, feet	0.40
Airfoil section, parallel to stream	NACA 65006
Gap between tail and fuselage at 0° deflection, inches	1/16
Vertical tail (all-movable differentially, pivoting about axis perpendicular to longitudinal axis of model)	
Area (including 1.4 square feet included in fuselage), square feet	3.3
Aspect ratio	5.0
Taper ratio	0.22
Sweepback, quarter-chord line, degrees	45
Span, feet	4.05
Mean aerodynamic chord (including area included in in fuselage), feet	0.93
Leading edge of mean aerodynamic chord	Station 151.0
Root chord, feet	1.34
Tip chord, feet	0.29
Airfoil section, perpendicular to quarter-chord line	NACA 65009
Gap between tail and fuselage at 0° deflection, inches	1/16
Fuselage	
Fineness ratio	12.4
Ordinate at station x (x = 8.0 to x = 139.4), inches	$r = 8.5\left[1 - \left(\frac{x}{102} - 1\right)^2\right]^{3/4}$

[redacted]

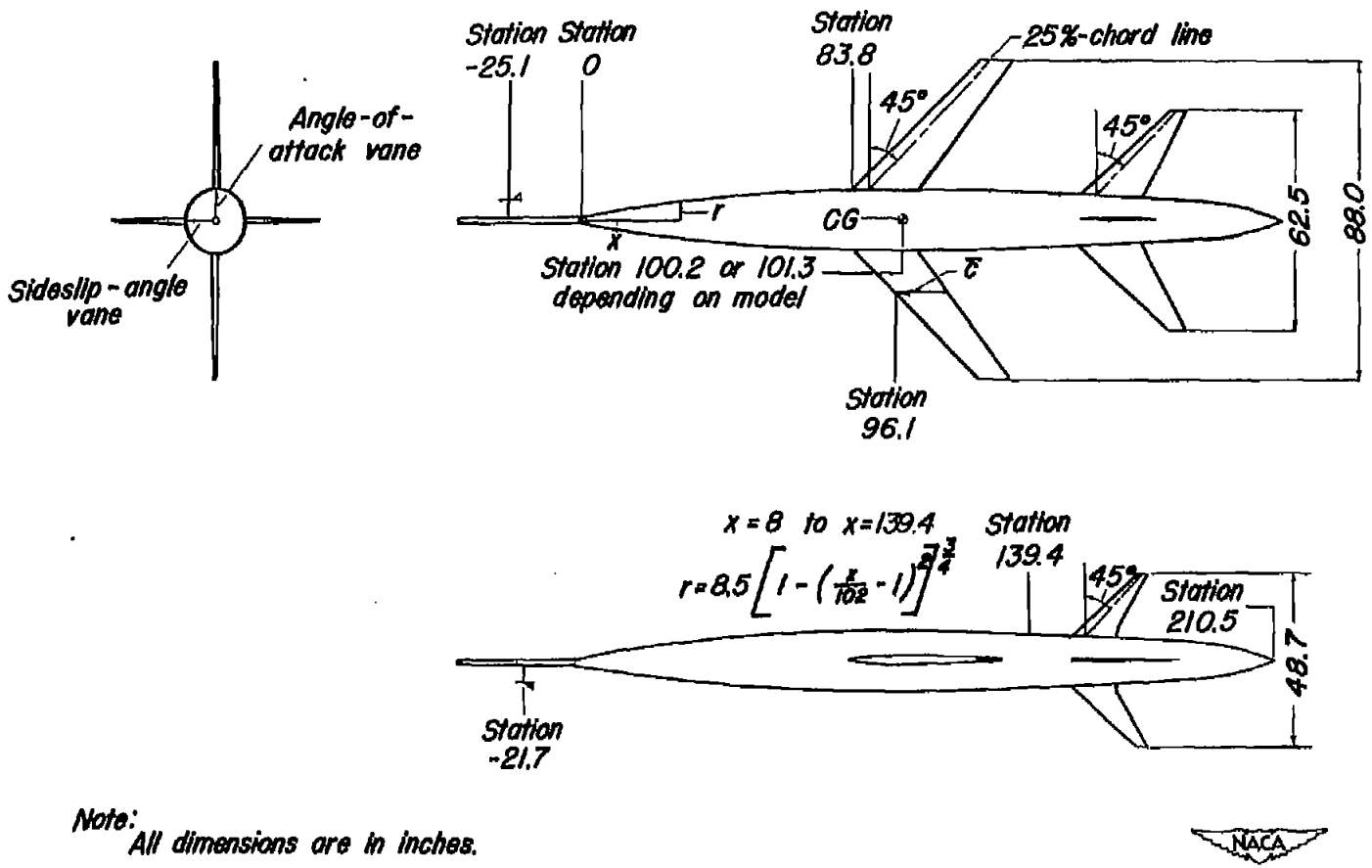

Figure 1.- Three-view drawing of free-fall model.

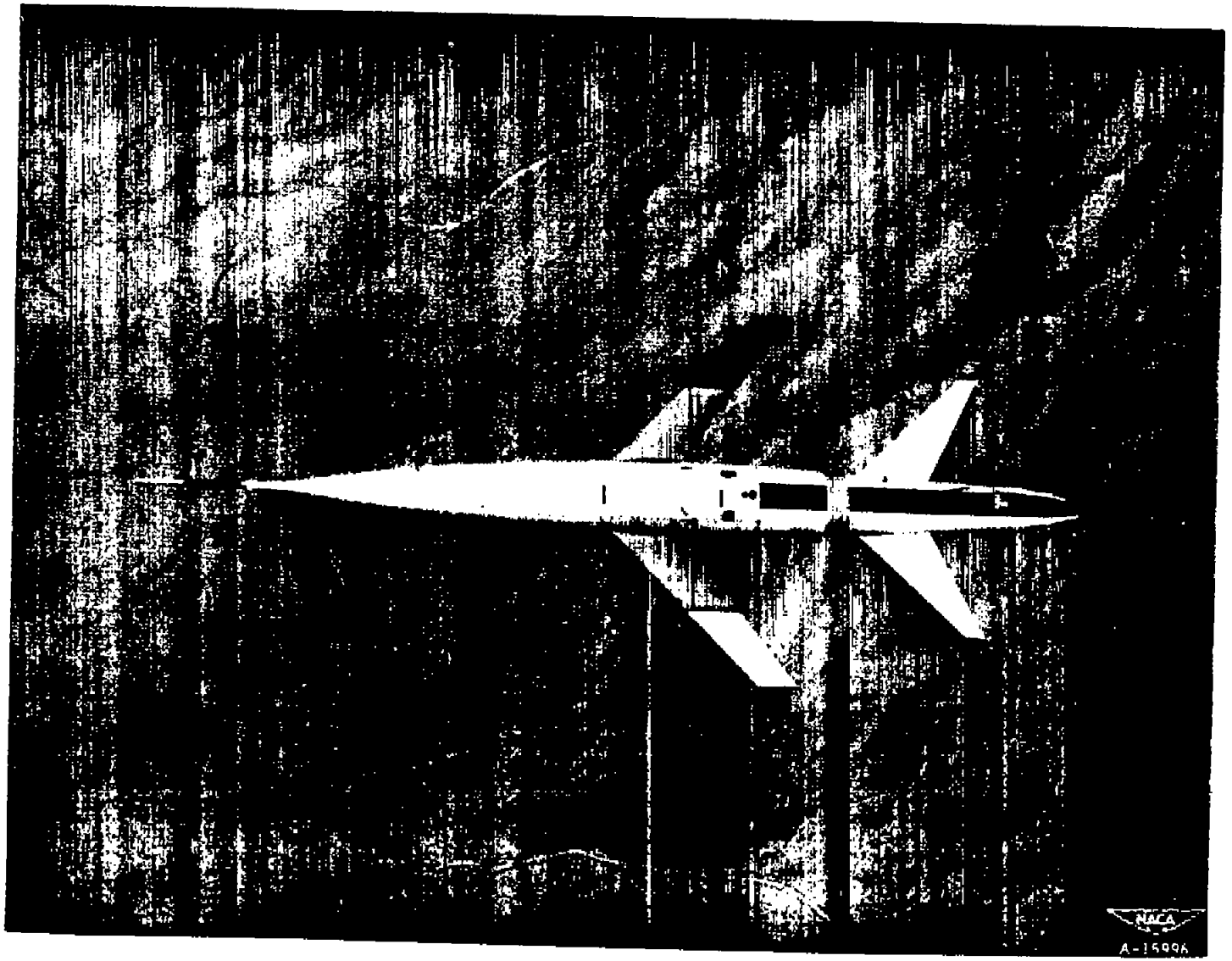

Figure 2.- Model in free-fall immediately after release from drop airplane.

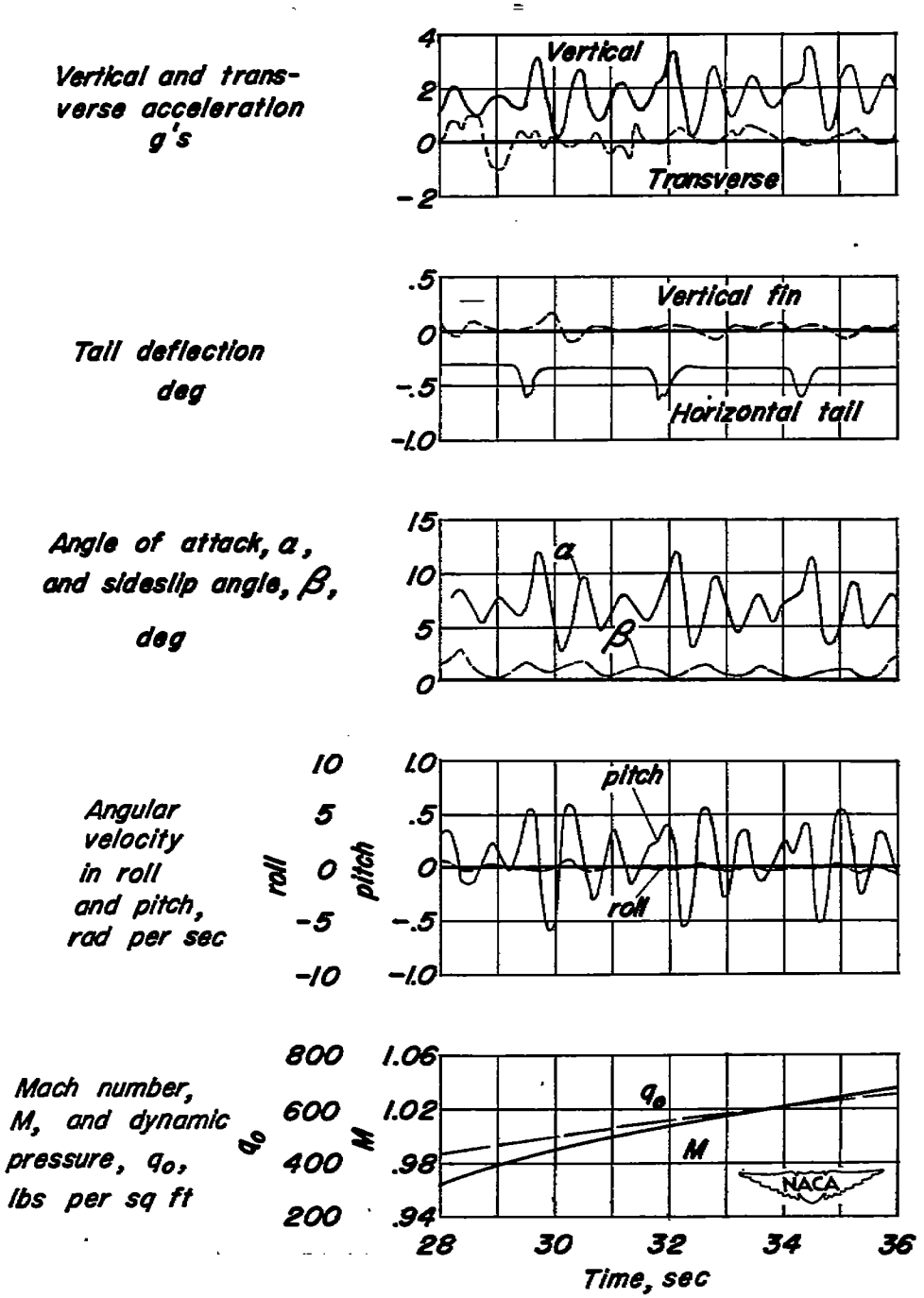

Figure 3.– Time history showing typical data obtained during oscillations of model.

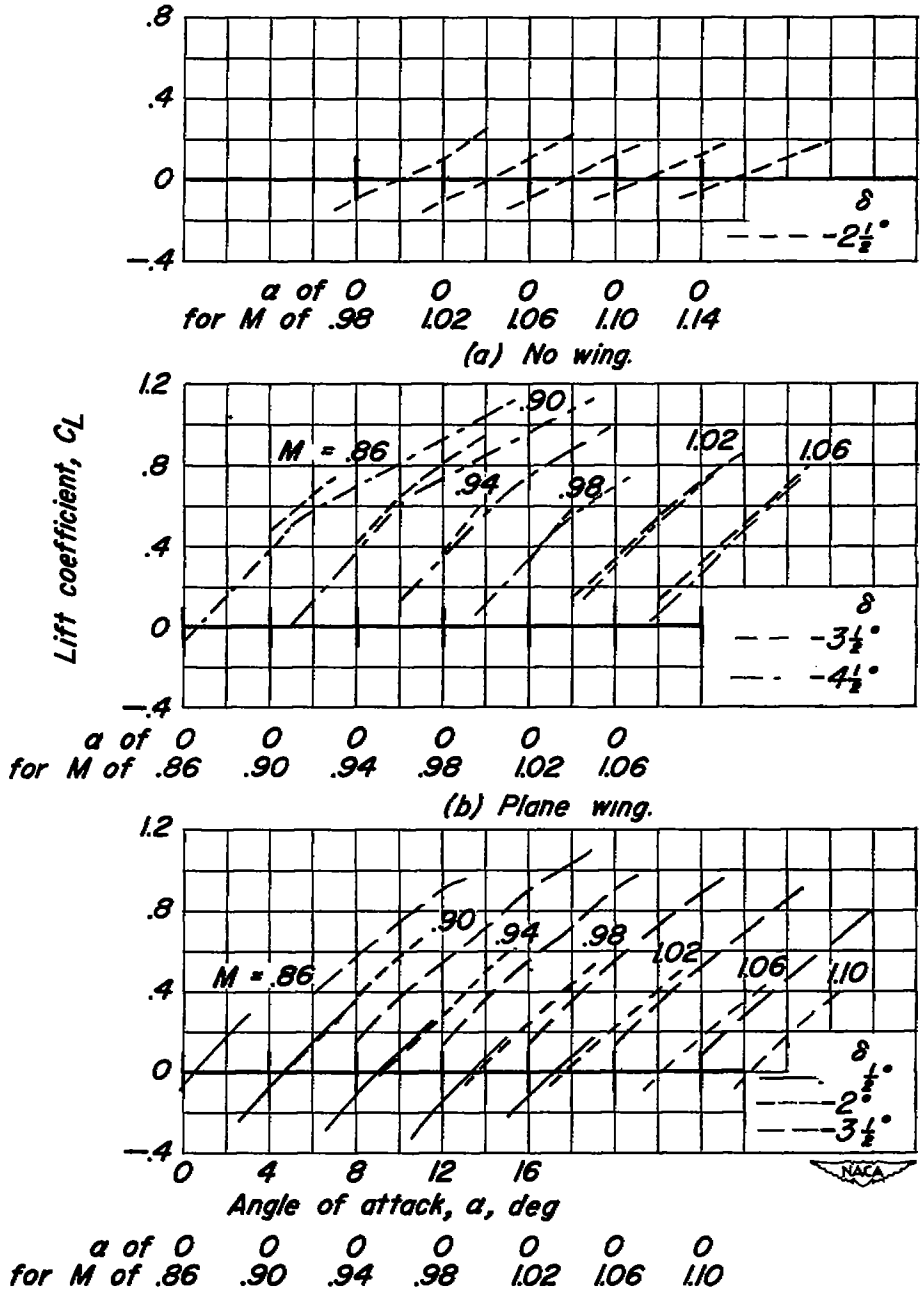

Figure 4.– Variation of lift coefficient with angle of attack for the test configurations at different Mach numbers and horizontal-tail deflections.

[redacted]

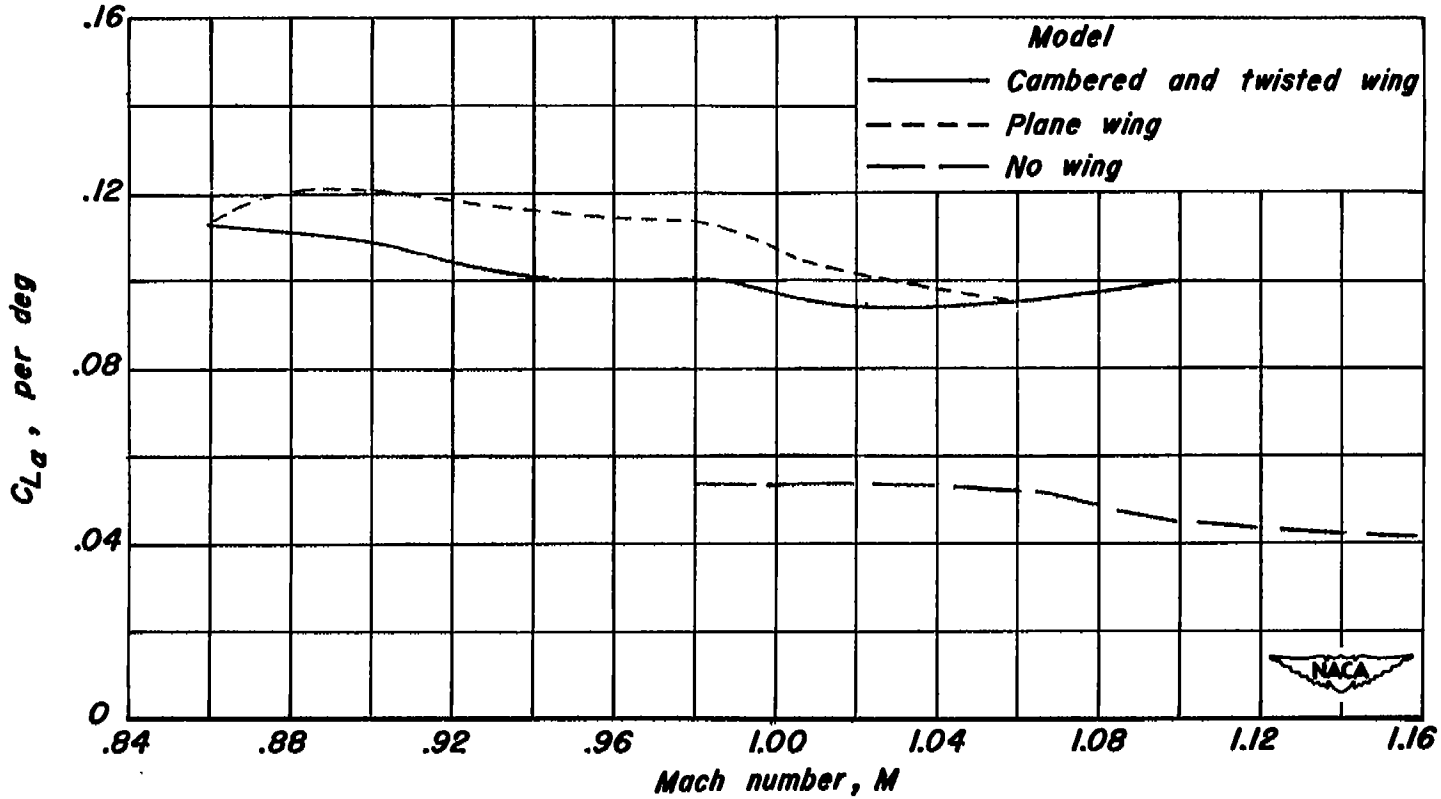

Figure 5.- Variation with Mach number of lift-curve slope, C_{L_α}, of complete model.

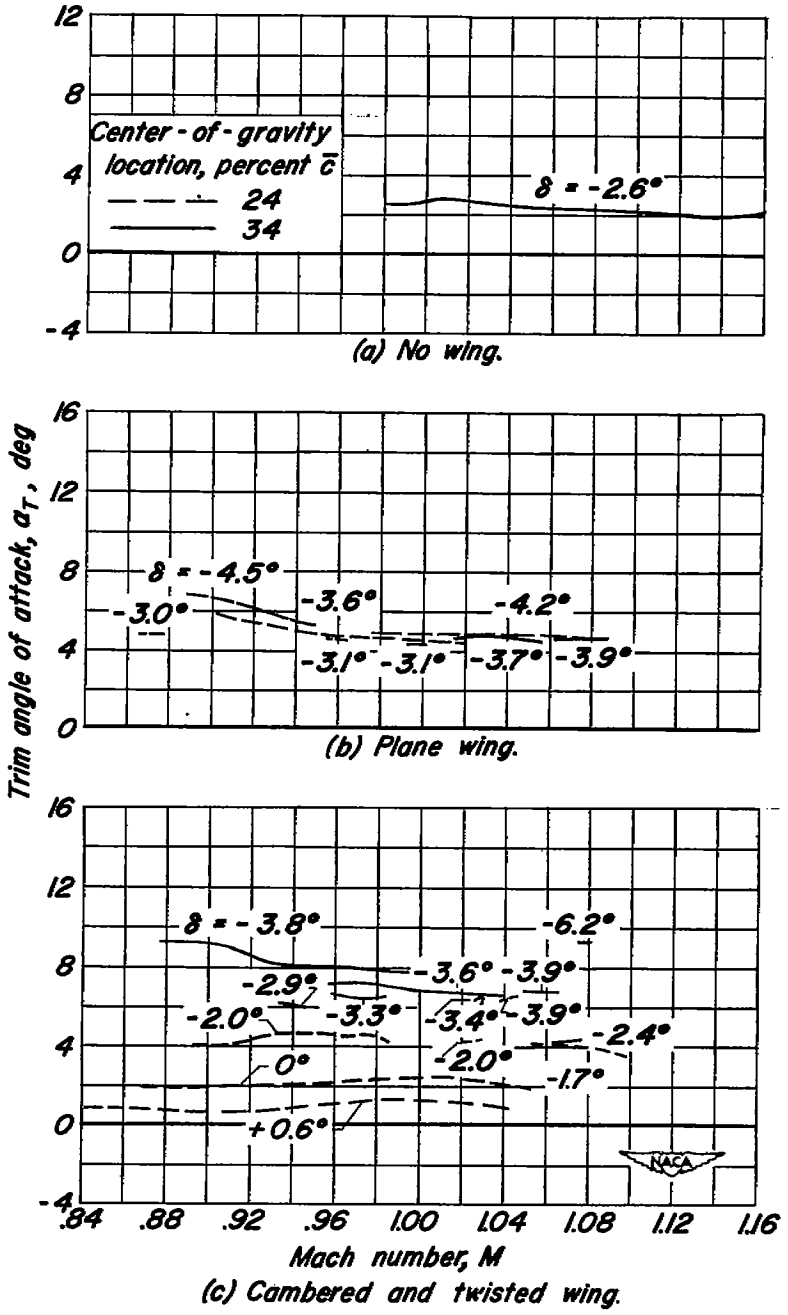

Figure 6.- Variation with Mach number of trim angles of attack for various horizontal-tail deflections for the test configurations.

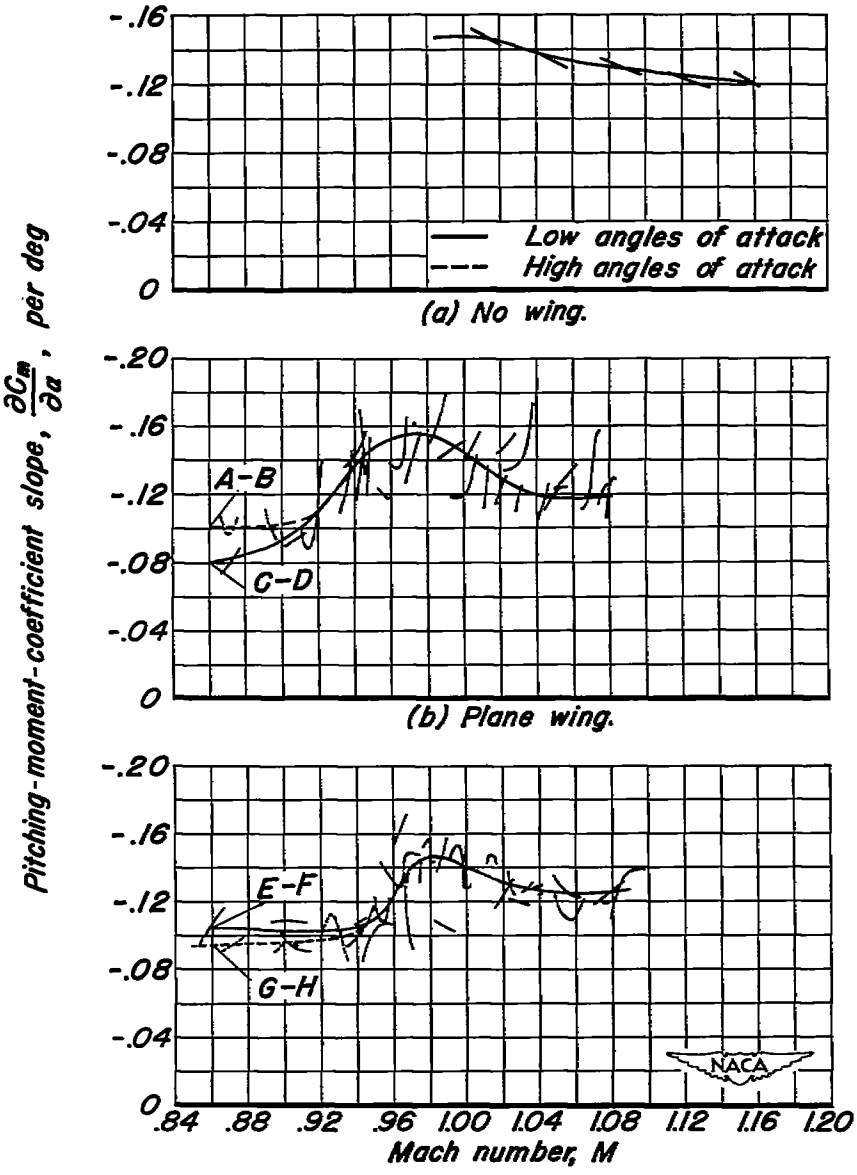

Figure 7. - Variation with Mach number of static stability parameter, $\frac{\partial C_m}{\partial \alpha}$, for the test configurations as determined from fixed - control oscillations. Center of gravity at 0.24 $\bar{c}$.

[redacted]

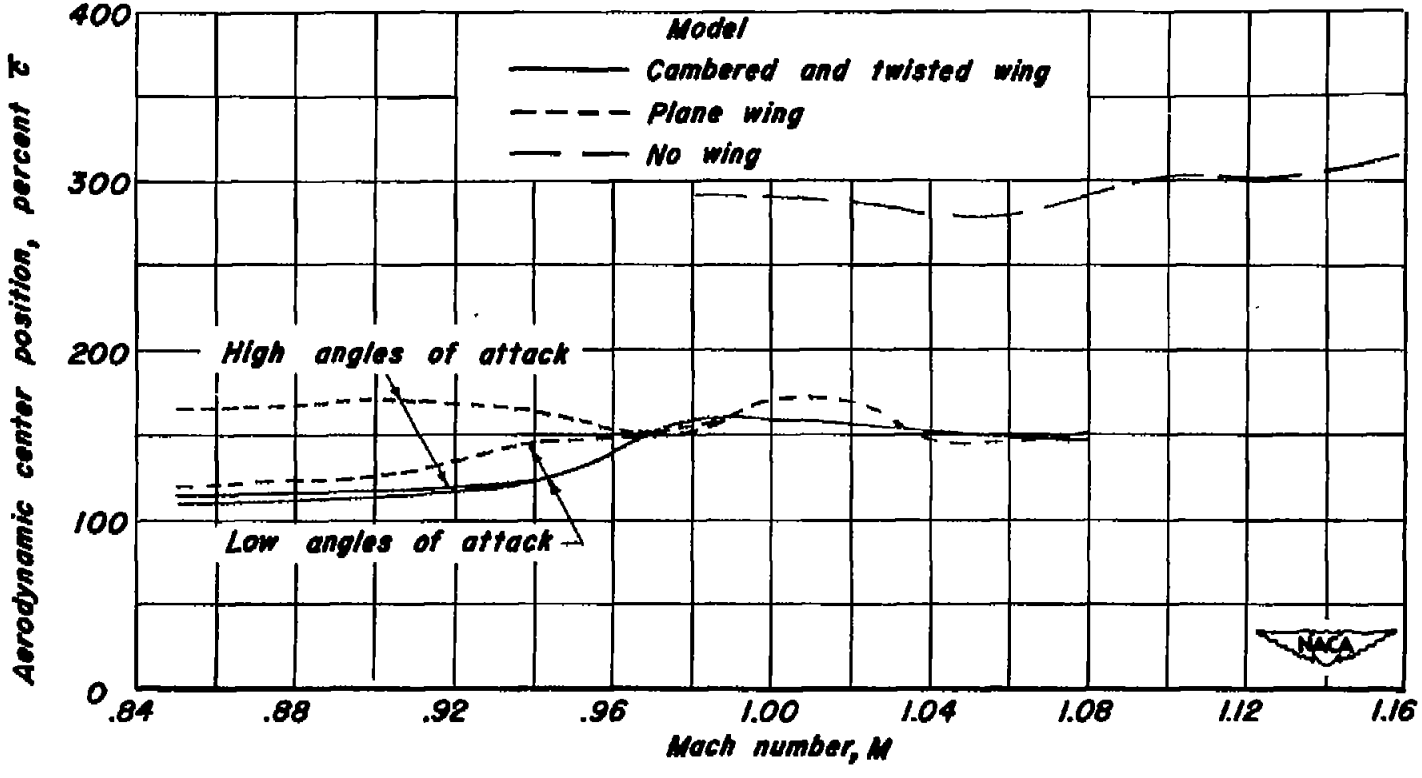

Figure 8. - Variation with Mach number of aerodynamic center position of complete model.

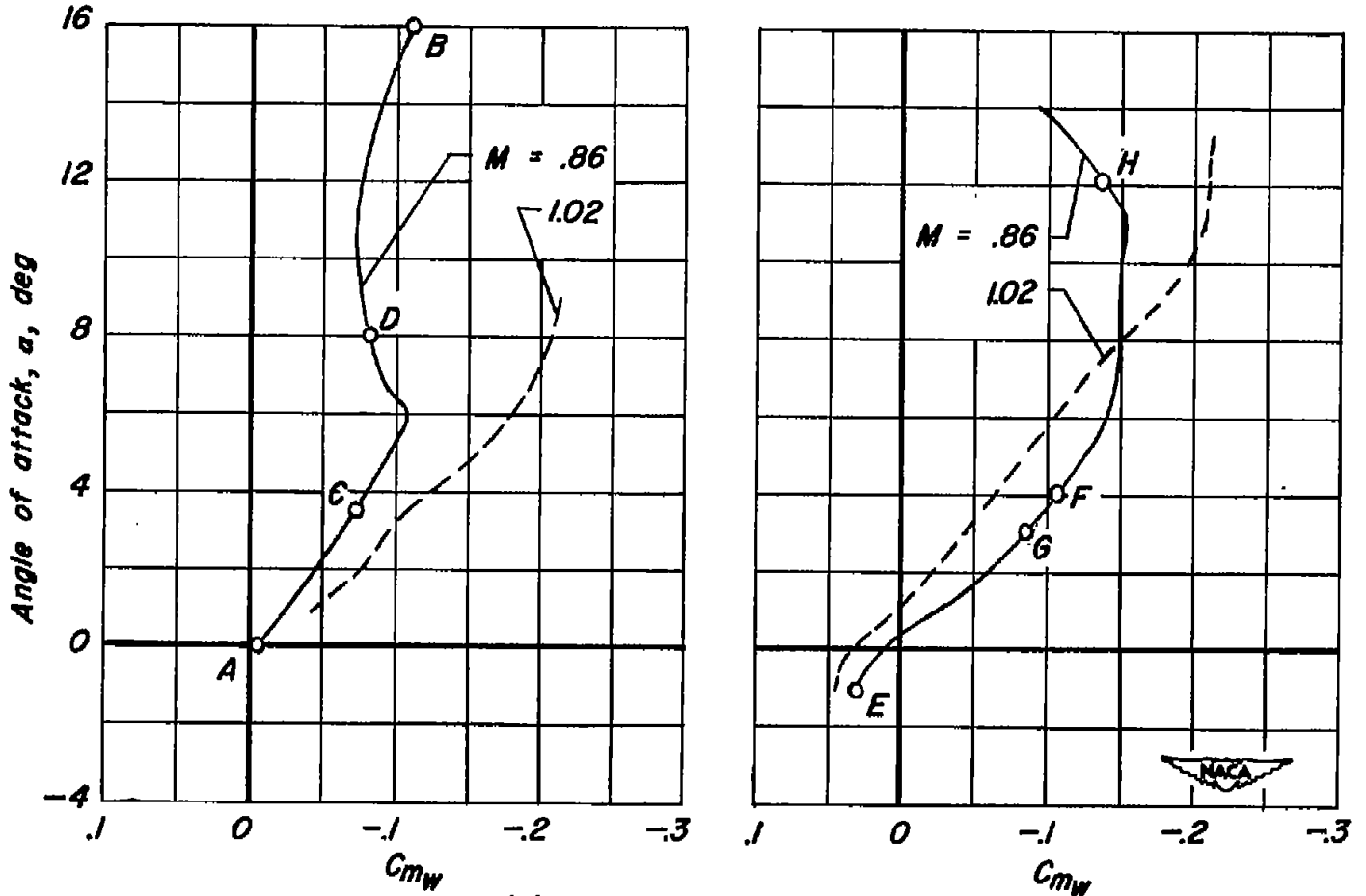

(a) Plane-wing model.

(b) Cambered-and twisted-wing model.

Figure 9.- Variation with angle of attack of the pitching-moment coefficients of the exposed wing panels for the wing-on models.

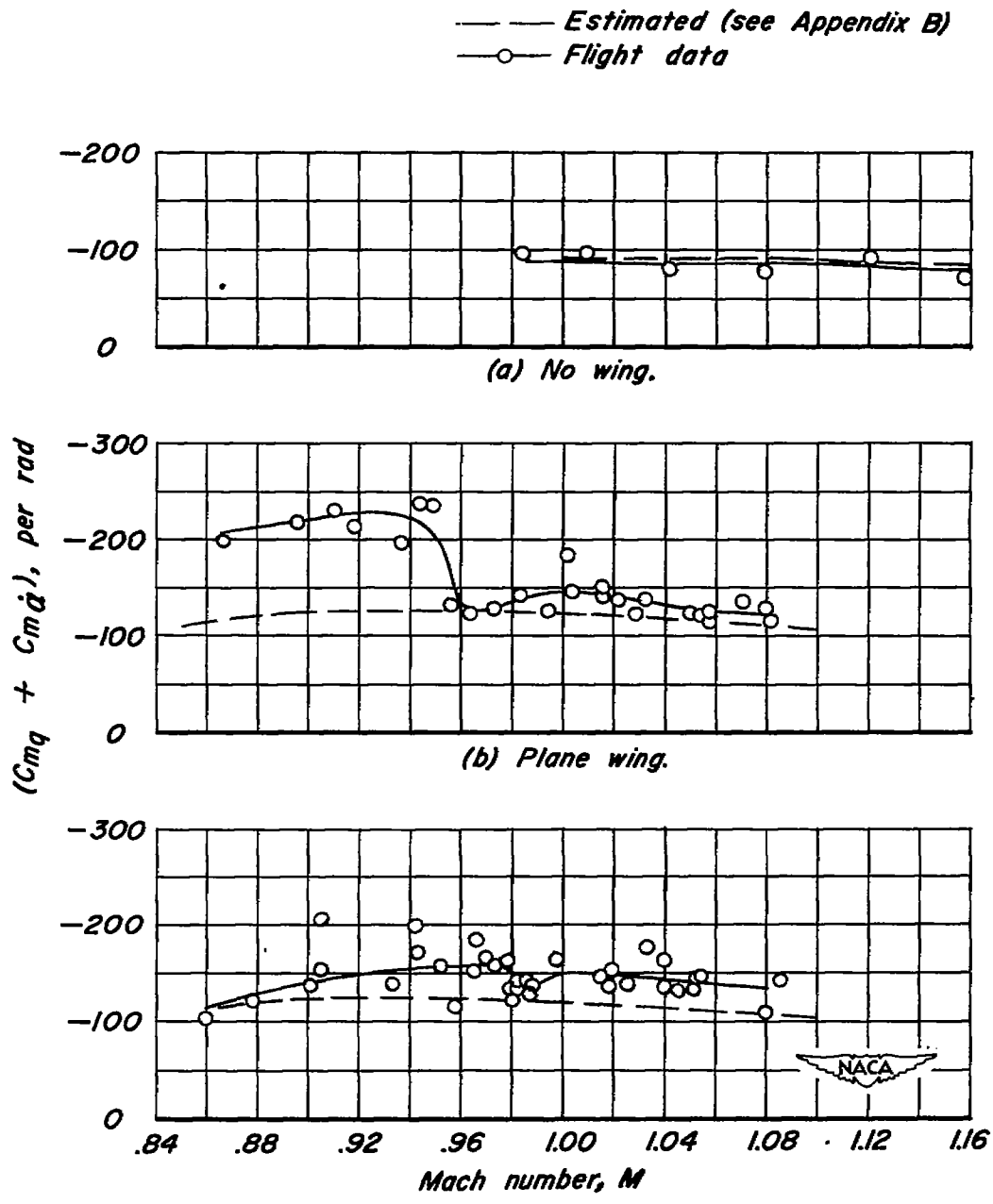

Figure 10.- Variation with Mach number of damping factor $(C_{m_q} + C_{m_{\dot{\alpha}}})$ for three models.

[redacted]

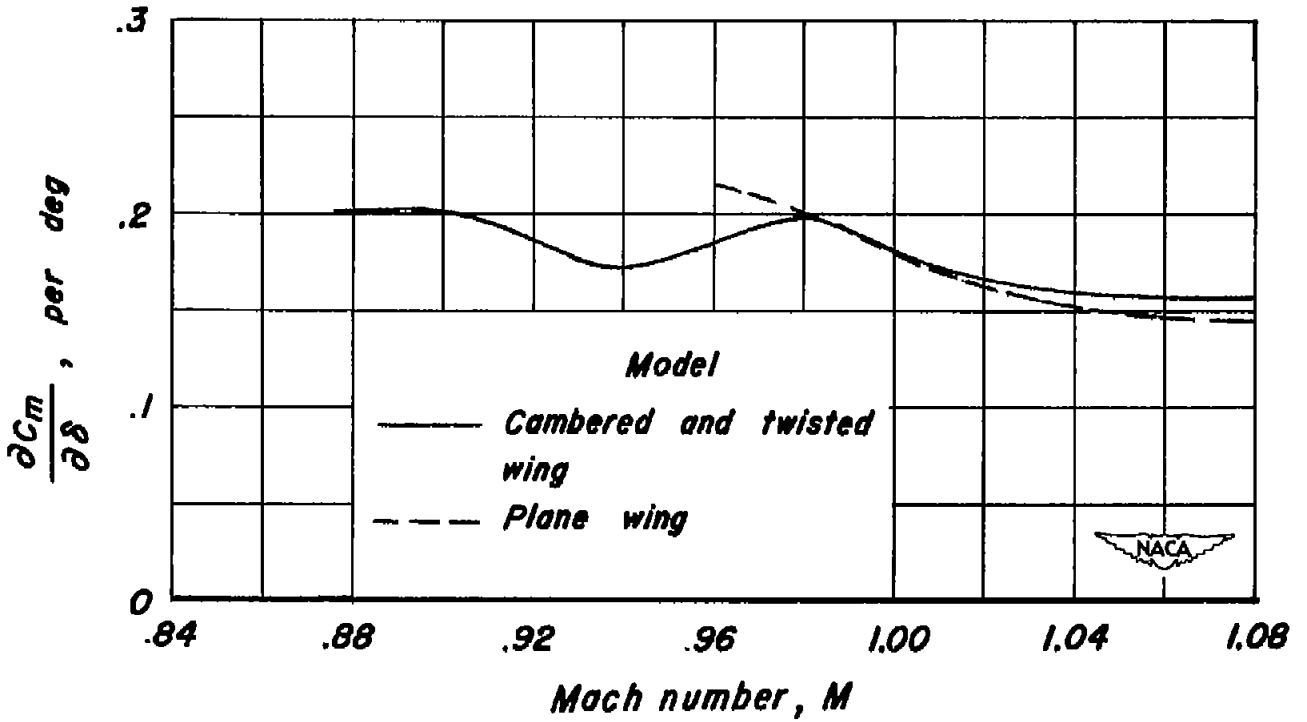

Figure 11.- Variation with Mach number of horizontal-tail-effectiveness parameter, $\frac{\partial C_m}{\partial \delta}$.

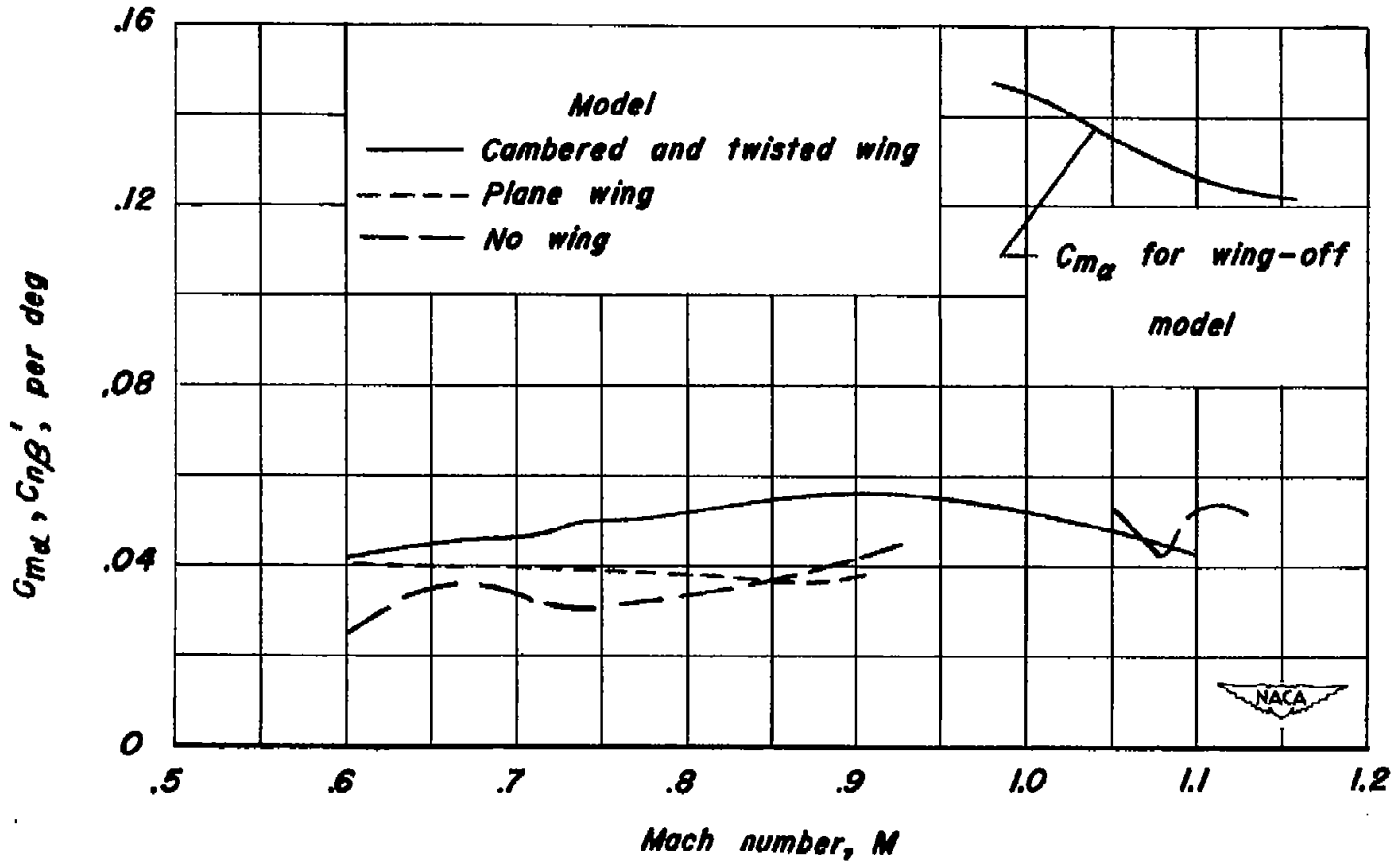

Figure 12.- Variation with Mach number of the static stability parameter, C_{n_β}', for the test configurations. (C_{n_β}' based on $S\bar{c}$).

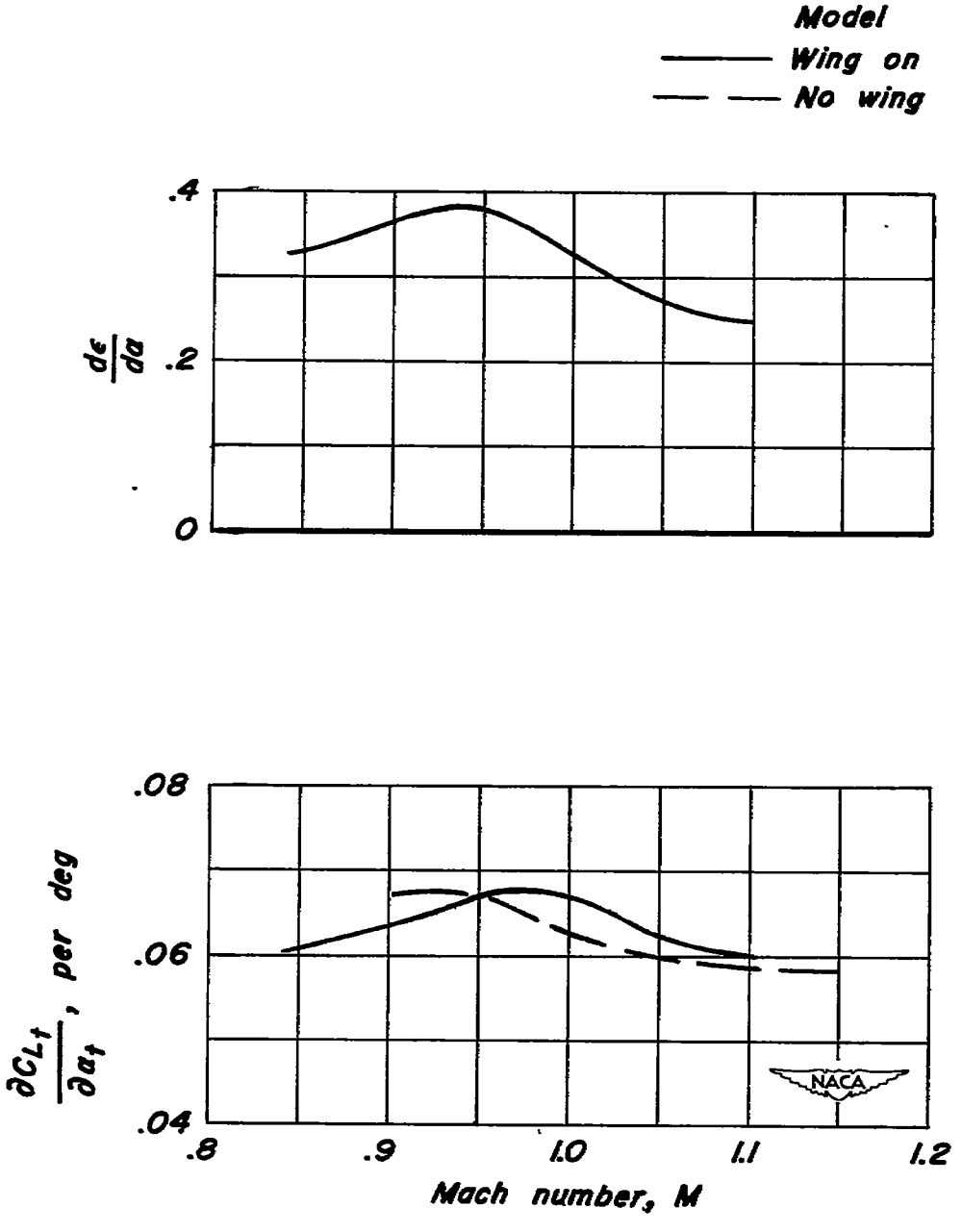

Figure 13.- Characteristics of models assumed in estimating values of $(C_{m_q} + C_{m_{\dot{\alpha}}})$.

NACA-Langley - 8-29-52 - 400